Available online at www.sciencedirect.com

ScienceDirect

Ceramics International 40 (2014) 199–202

CERAMICS INTERNATIONAL

www.elsevier.com/locate/ceramint

Ferroelectric properties of $BiFeO_3$ nanodots shattered by atomic force microscope

J.Y. Son*, H. Song**

Department of Applied Physics, College of Applied Science, Kyung Hee University, Suwon 446-701, Republic of Korea

Received 22 April 2013; received in revised form 30 May 2013; accepted 30 May 2013
Available online 5 June 2013

Abstract

A $BiFeO_3$ (BFO) nanodot was deposited on a Nb-doped $SrTiO_3$ substrate by dip-pen nanolithography. The BFO nanodot had a diameter of about 50 nm after drying and annealing to remove the solvent contained in the nanodot. To make nanoparticles smaller than a few tens of nanometers, the BFO nanodot was then shattered using an atomic force microscope. Ferroelectric BFO nanodots smaller than 20 nm in diameter were successfully fabricated after the annealing process. A ferroelectric BFO nanodot smaller than 15 nm exhibited good ferroelectric properties with a canonical piezoelectric hysteresis loop and tunneling currents depending on ferroelectric polarizations.

Keywords: Ferroelectricity; $BiFeO_3$ nanodot; Shattering process; Atomic force microscopy

1. Introduction

Non-volatile random access memory (NVRAM) technology has been used in various memory devices such as flash memories, magnetic random access memory, resistive RAM, phase-change RAM and ferroelectric RAM (FeRAM) [1–7]. To store information, these memory devices utilize different storage concepts that use electrical charge, magnetization, resistance, and ferroelectric polarization [1–6]. In particular, scaling down has made it possible to maximize the storage density and to enhance the speed of memory [8,9]. For this reason, many researchers have studied nanoscale NVRAMs consisting of nanomaterials such as nanowires, nanotubes, and nanodots.

FeRAMs using ferroelectric polarization for information storage have attracted researchers because they have a simple device structure consisting of one ferroelectric capacitor and one transistor [1].There are several methods, such as self-assembly, nanotemplates, and dip-pen lithography processes, to form ferroelectric nanostructures of nanowires, nanotubes, and nanodots, although conventional photolithography techniques are not applicable [10–15]. The self-assembly process produces very small nanodots, less than a few nanometers in diameter, but the self-assembled nanodots are randomly positioned. In contrast with the self-assembly process, the nanofabrication process using nanotemplates such as anodic aluminum oxide (AAO) produces well-aligned nanostructures, though they are bigger than those generated by self-assembly [12]. However, it is hard to make nanoscale FeRAMs using the well-aligned nanostructures obtained by the AAO technique. The dip-pen lithography technique, on the other hand, has the merit of controlling the position and size of nanostructures [13,15]. In this study, we investigated the ferroelectric properties of $BiFeO_3$ (BFO) nanodots on an Nb-doped $SrTiO_3$ substrate deposited by dip-pen lithography. We formed a BFO nanodot smaller than 15 nm that exhibited good ferroelectric properties confirmed by conducting atomic force microscopy (CAFM) and piezoresponse force microscopy (PFM).

2. Experimental procedure

Fig. 1 shows schematic drawings of the shattering process for a dip-pen lithography BFO nanodot. To improve upon the dip-pen lithography process, we also used an Nb-doped $SrTiO_3$ substrate, which had an atomically flat surface with well-aligned terraces formed by HF treatment with annealing [16].To make an atomically flat surface on the Nb-doped $SrTiO_3$ substrates (Nb doping level ~1 wt% and resistivity ~0.001 Ω cm), which can be used as a bottom electrode, the Nb-doped $SrTiO_3$ substrates were dipped

*Corresponding author. Tel.: +82 31 201 3770; fax: +82 31 204 8122.
**Corresponding author.
E-mail addresses: jyson@khu.ac.kr (J.Y. Son), hson@khu.ac.kr (H. Song).

0272-8842/$ - see front matter © 2013 Elsevier Ltd and Techna Group S.r.l. All rights reserved.
http://dx.doi.org/10.1016/j.ceramint.2013.05.123

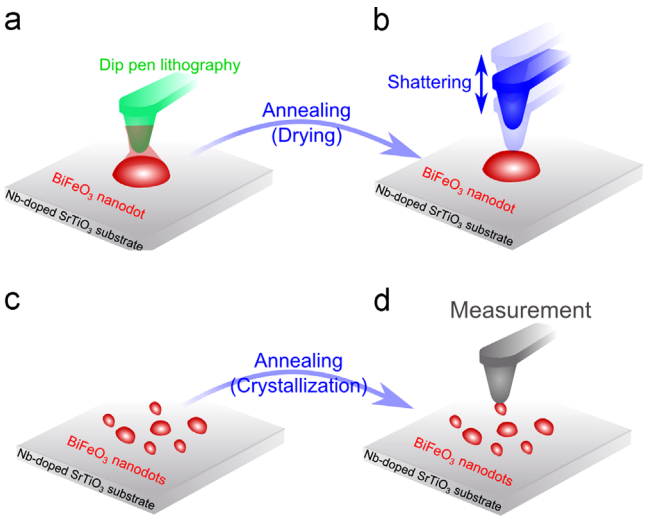

Fig. 1. Schematic drawings of the shattering process for a BFO nanodot. (a) The formation of a BFO nanodot on an Nb:STO substrate by dip-pen lithography. (b) The shattering of a BFO nanodot using an AFM tip. (c) Shattered BFO nanodots on the Nb:STO substrate. (d) Crystallized BFO nanodots after the annealing process for the crystallization of the shattered PTO nanodots.

in a dilute HF solution and annealed at 1000 °C for 1 h. Then, a BFO nanodot was deposited on a Nb-doped $SrTiO_3$ (Nb:STO) substrate by dip-pen lithography, where the sizes of the nanodots were controlled by suitably adjusting the dip-pen deposition time. Then, the BFO nanodot was immediately dried by an annealing process (at 200 °C for1 h) and it was shattered by AFM, as shown in Fig. 1(b) and (c). For the shattering process, we used a diamond AFM tip with a radius of 15 nm, an amplitude of 100 nm, and a shattering frequency of 75 kHz. Before the shattering process, the AFM tip was contacting with the top of the BFO nanodot. Then, the AFM tip was vibrated to shatter the BFO nanodot. After the shattering process, we annealed the shattered BFO nanodots for crystallization at 600 °C for 1 h, because the shattered BFO nanodots have a crystallization temperature above 300 °C and thus were not yet crystallized [17].

3. Results and discussion

Fig. 2(a) shows the AFM image of the BFO nanodot created by dip-pen lithography on the Nb:STO substrate. In the bottom background region, the well-aligned terraces of the Nb:STO substrate are discernible where the Nb:STO substrate was used as the bottom electrode of the BFO nanodot-capacitor. The Nb:STO substrate had an atomically flat surface with a surface roughness of less than 0.2 nm. We roughly estimated the diameter of the BFO nanodot to be about 50 nm. It is hard to observe the BFO nanodot in the PFM image, as shown in Fig. 2(b),because it is not crystallized. We could then perform a shattering process to cleave the BFO nanodot into small BFO shatters (Fig. 2c). The BFO nanodot with a diameter of ~50 nm was cleaved into numerous BFO nanoparticles (nanodots) with diameters smaller than 15 nm. For the crystallization, the shattered BFO nanodots were annealed at 600 °C for 1 h. Finally, after the crystallization process, the ferroelectric properties of the shattered BFO nanodots were analyzed by PFM experiments that consisted of switching the ferroelectric polarizations and measuring the PFM signals and piezoelectric hysteresis loops.

Fig. 3(a) shows a PFM image of the shattered BFO nanodots after the crystallization process. This image exhibits a significantly enhanced PFM signal compared to that of the non-crystalline BFO nanodot (Fig. 2b), indicating that the BFO nanodots were sufficiently crystallized. The PFM image reveals that the BFO nanodots have randomly oriented polarizations. To examine the ferroelectric switching behavior, we performed PFM switching experiments for the BFO nanodot marked in Fig. 2(d). This BFO nanodot had a diameter of ~15 nm and a thickness of ~8 nm. We easily modified the ferroelectric polarizations of the BFO nanodot so that it possessed different directions of up and down polarization by applying positive and negative biases of 2 V to the conducting AFM tip. Fig. 3(b) and (c) shows PFM images of the BFO nanodot after the switching process with biases of +2 V and −2 V, respectively. The small BFO nanodot exhibited well-switched ferroelectric domains along the upward and downward directions, indicating that this small BFO nanodot had good ferroelectric properties. For the BFO nanodots with diameters less than 15 nm, it was difficult to switch the ferroelectric polarizations using PFM due to high leakage currents.

We also obtained a typical piezoelectric hysteresis loop for the small BFO nanodot using PFM with a measurement frequency of 10 kHz (Fig. 4d). There were small shifts in the hysteresis loop due to imprinting effects resulting from the asymmetric electrode configuration of the conducting AFM tip, the BFO nanodot, and the Nb:STO substrate. The hysteresis loop of the BFO nanodot shows a coercive voltage of about 0.6 V and an effective remnant piezoelectric constant of about 40 pm/V. In previous studies of ferroelectric $PbTiO_3$ (PTO) nanodots, the 60 and 40 nm PTO nanodots exhibited piezoelectric constants that were 100 pm/V larger than that of the small BFO nanodot [12,13]. It is notable that a small BFO nanodot with a diameter less than 15 nm has good ferroelectric properties with a canonical piezoelectric hysteresis loop.

We further investigated the tunneling current characteristics of the small BFO nanodot depending on its ferroelectric polarizations of upward and downward directions (Fig. 4). Fig. 4(a) shows the tunneling current curves as a function of applied voltage depending on the upward and downward ferroelectric polarizations. The tunneling current curves are clearly distinguished according to their directions of ferroelectric polarization. The polarization-dependent tunneling current can be explained using a model of a ferroelectric tunnel junction with a trapezoidal tunneling barrier [18]. The slope of the tunneling barrier depends on the change in the electrostatic potential associated with the ferroelectric polarization reversal and the resulting reorientation of the depolarization field. In other words, the small BFO nanodot exhibited two distinct resistance states, the high resistance state (HRS: downward polarization) and the low resistance state (LRS: upward polarization). We also confirmed that the difference in LRS and HRS is reproducible for up to 200 cycles, as shown in

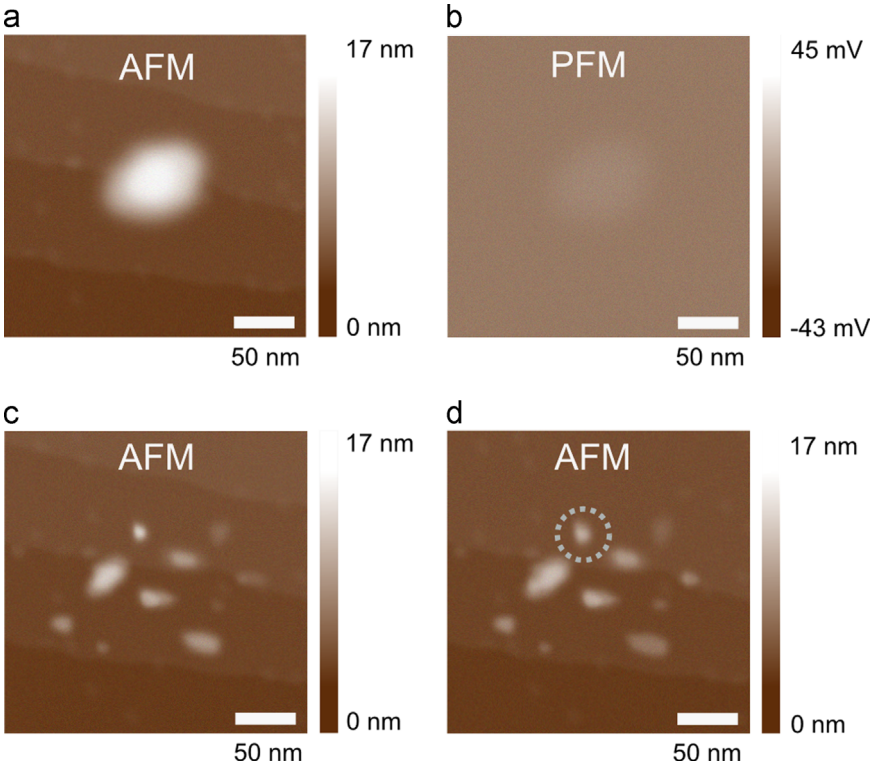

Fig. 2. (a) AFM image of a BFO nanodot formed by dip-pen lithography on the Nb-doped STO substrate and annealed (200 °C for 1 h). The BFO nanodot has a diameter of about 50 nm and terraces can be observed on the Nb-doped STO substrate. (b) PFM image of the same BFO nanodot on the Nb:STO substrate as shown in (a). (c) AFM image after the shattering of the BFO nanodot shown in (a). (d) AFM image of the shattered PTO nanodots after the annealing (600 °C for 1 h) for crystallization.

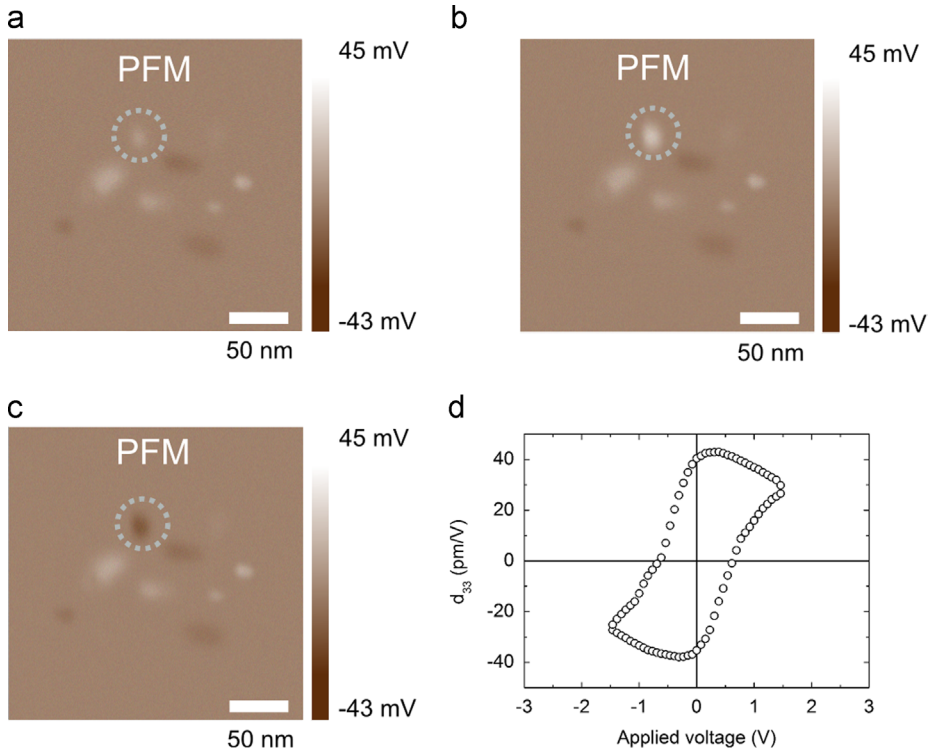

Fig. 3. (a) PFM image of the shattered BFO nanodots shown in Fig. 2(d). (b), (c) PFM images of the BFO nanodot (marked in Fig. 2d) smaller than 15 nm after the switching process with biases of (b) +2 V and (c) −2 V. (e) Piezoelectric hysteresis loop of the BFO nanodot.

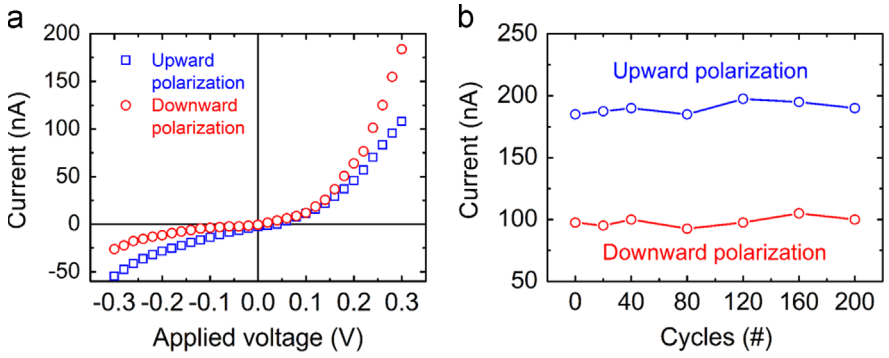

Fig. 4. (a) Tunneling current curves as a function of applied voltage depending on the upward and downward ferroelectric polarizations of the BFO nanodot smaller than 15 nm. (b) Tunneling current curve as a function of switching cycles depending on the upward and downward ferroelectric polarizations of the BFO nanodot.

Fig. 4(d). Thus, we suggest that the small BFO nanodot is suitable for use in FeRAMs or logic devices.

4. Conclusion

A BFO nanodot was formed by dip-pen nanolithography on a Nb-doped $SrTiO_3$ substrate using a BFO precursor sol. After the drying and annealing processes, we obtained a gel BFO nanodot with a diameter of about 50 nm. This nanodot was then shattered into dots of various sizes, ranging from several nanometers to a few tens of nanometers, using an atomic force microscope. After crystallization, the ferroelectric BFO nanodots with diameters less than 15 nm exhibited good ferroelectric properties, which were confirmed by CAFM and PFM.

Acknowledgments

The research was supported by the National Research Foundation of Korea Grant funded by the Korea Government (No. 2012R1A2A2A01046451).

References

[1] J.F. Scott, C.A.P.D. Araujo, Ferroelectric memories, Science 246 (1989) 1400–1405.
[2] J.H. Cho, S.J. Kim, Y.S. Yang, Structural change in $Bi_4(Si_xGe_{1-x})_3O_{12}$ glasses during crystallization, Solid State Communications 119 (7) (2001) 465–470.
[3] H.-B.-R. Lee, G.H. Gu, J.Y. Son, C.G. Park, H. Kim, Spontaneous formation of vertical magnetic-metal-nanorod arrays during plasma-enhanced atomic layer deposition, Small 4 (2008) 2247–2254.
[4] J. Park, C.W. Ahn, I.W. Kim, Photocurrent of lead-free $(K_{0.5}Na_{0.5})(Mn_{0.0005}Nb_{0.995})O_3$, Journal of Applied Physics 112 (2012) 014312.
[5] G.H. Kim, J.H. Lee, Y. Ahn, W. Jeon, S.J. Song, J.Y. Seok, J.H. Yoon, K.J. Yoon, T.J. Park, C.S. Hwang, 32×32 crossbar array resistive memory composed of a stacked Schottky diode and unipolar resistive memory, Advanced Functional Materials 23 (11) (2013) 1440–1449.
[6] F. Xiong, M.-H. Bae, Y. Dai, A.D. Liao, A. Behnam, E.A. Carrion, S. Hong, D. Ielmini, E. Pop, Self-aligned nanotube-nanowire phase change memory, Nano Letters 13 (2) (2013) 464–469.
[7] N. Jeon, D. Rout, I.W. Kim, S.-J.L. Kang, Enhanced multiferroic properties of single-phase $BiFeO_3$ bulk ceramics by Ho doping, Applied Physics Letters 98 (2011) 072901.
[8] I. Jung, J.Y. Son, A nonvolatile memory device made of a graphene nanoribbon and a multiferroic $BiFeO_3$ gate dielectric layer, Carbon 50 (10) (2012) 3854–3858.
[9] J.Y. Son, S. Ryu, Y.-C. Park, Y.-T. Lim, Y.-S. Shin, Y.-H. Shin H.M. Jang, A nonvolatile memory device made of a ferroelectric polymer gate nanodot and a single-walled carbon nanotube, ACS Nano 4 (12) (2012) 7315–7320.
[10] H. Zheng, J. Wang, S.E. Lofland, Z. Ma, L. Mohaddes-Ardabili, T. Zhao, L. Salamanca-Riba, S.R. Shinde, S.B. Ogale, F. Bai, D. Viehland, Y. Jia, D.G. Schlom, M. Wuttig, A. Roytburd, R. Ramesh, Multiferroic $BaTiO_3$–$CoFe_2O_4$ nanostructures, Science 303 (5658) (2004) 661–663.
[11] J.F. Scott, Applications of modern ferroelectrics, Science 315 (2007) 954–959.
[12] W. Lee, H. Han, A. Lotnyk, M.A. Schubert, S. Senz, M. Alexe, D. Hesse, S. Baik, U. Gosele, Individually addressable epitaxial ferroelectric nanocapacitor arrays with near Tb inch-2 density, Nature Nanotechnology 3 (7) (2008) 402–407.
[13] J.Y. Son, Y.-H. Shin, S. Ryu, H. Kim, H.M. Jang, Dip-pen lithography of ferroelectric $PbTiO_3$ nanodots, Journal of the American Chemical Society 131 (41) (2009) 14676–14678.
[14] Y. Kim, H. Han, Y. Kim, W. Lee, M. Alexe, S. Baik, J.K. Kim, Ultrahigh density array of epitaxial ferroelectric nanoislands on conducting substrates, Nano Letters 10 (6) (2010) 2141–2146.
[15] I. Jung, J.Y. Son, Dip-pen lithography of $BiFeO_3$ nanodots, Journal of the American Ceramic Society 95 (2012) 3716–3718.
[16] M. Kawasaki, K. Takahashi, T. Maeda, R. Tsuchiya, M. Shinohara, O. Ishiyama, T. Yonezawa, M. Yoshimoto, H. Koinuma, Atomic control of the $SrTiO_3$ crystal surface, Science 266 (5190) (1994) 1540–1542.
[17] Y.-H. Lee, J.-M. Wu, Y.-L. Chueh, L.-J. Chou, Low-temperature growth and interface characterization of $BiFeO_3$ thin films with reduced leakage current, Applied Physics Letters 87 (17) (2005) 172901–172903.
[18] W.F. Brinkman, R.C. Rynes, J.M. Rowell, Tunneling conductance of asymmetrical barriers, Journal of Applied Physics 41 (1970) 1915–1921.